

## REVEALING THE WARM-HOT INTERGALACTIC MEDIUM WITH OVI ABSORPTION

Renyue Cen, Todd M. Tripp, Jeremiah P. Ostriker, and Edward B. Jenkins

Princeton University Observatory, Princeton University, Princeton, NJ 08544

cen@astro.princeton.edu, tripp@astro.princeton.edu

jpo@astro.princeton.edu, ebj@astro.princeton.edu

Draft version March 19, 2024

## ABSTRACT

Hydrodynamic simulations of growth of cosmic structure suggest that 30-50% of the total baryons at  $z = 0$  may be in a warm-hot intergalactic medium (WHIM) with temperatures  $10^5 - 10^7$  K. The O VI 1032, 1038 absorption line doublet in the FUV portion of QSO spectra provides an important probe of this gas. Utilizing recent hydrodynamic simulations, it is found that there should be 5 O VI absorption lines per unit redshift with equivalent widths 35 mÅ, decreasing rapidly to 0.5 per unit redshift at 350 mÅ. About 10% of the total baryonic matter or 20-30% of the WHIM is expected to be in the O VI absorption line system with equivalent width 20 mÅ; the remaining WHIM gas may be too hot or have too low metallicity to be detected in O VI. We find that the simulation results agree well with observations with regard to the line abundance and total mass contained in these systems. Some of the O VI systems are collisionally ionized and some are photoionized, but most of the mass is in the collisionally ionized systems. We show that the gas that produces the O VI absorption lines does not reside in virialized regions such as galaxies, groups, or clusters of galaxies, but rather has an overdensity of 10-40 times the average density. These regions form a somewhat connected network of filaments. The typical metallicity of these regions is  $0.1 - 0.3 Z_\odot$ .

Subject headings: Cosmology: large-scale structure of Universe { cosmology: theory { intergalactic medium { quasars: absorption lines { numerical method

## 1. INTRODUCTION

Three independent observations at  $z \sim 2$ , namely the latest cosmic microwave background experiments (Netterfield et al. 2001) at  $z > 2$ , the Lyman alpha forest decrement measurements (Rauch et al. 1997; Weinberg et al. 1997) at  $z \sim 2-3$ , and the deuterium-to-hydrogen ratio measurements (interpreted within the context of the standard nucleosynthesis theory, Burles & Tytler 1998), all consistently give  $\Omega_b(z=2) = (0.019 \pm 0.002)h^2 = 0.039 \pm 0.004$  (where  $h = H_0/100 \text{ km sec}^{-1} \text{ Mpc}^{-1} = 0.7$  is used for the last equality). On the other hand, in our local universe all the well-measured baryonic components do not appear to add up to the indicated baryonic density seen at high redshift by a factor of about three (e.g., Fukugita, Hogan, & Peebles 1998) with  $\Omega_b(z=0) = \Omega_{HI} + \Omega_{H_2} + \Omega_{X\text{-ray/cl}} = 0.0068 \pm 0.011$  (2 limit), where  $\Omega_{HI}$ ,  $\Omega_{H_2}$  and  $\Omega_{X\text{-ray/cl}}$  are the baryonic densities contained in stars, neutral atomic hydrogen detected in 21cm or damped Lyman alpha systems, molecular hydrogen and hot X-ray emitting gas in rich cluster centers. While a substantial amount of baryons may be in the low-redshift Ly forest with  $\Omega_{Ly} = 0.008$  (Penton, Shull, & Stocke 2000), it is still far short of accounting for the baryons seen at high redshift. Thus, most of the baryons are "missing" today.

Hydrodynamic simulations of structure growth suggest that a large fraction of the missing baryons at the present epoch may be in a gaseous phase with temperatures of  $10^5 - 10^7$  K at moderate overdensities, typically  $10-40$  (Cen et al. 1995; Cen & Ostriker 1999a; Davé et al. 2001). It is important to detect this gas to enable a better understanding of the baryon distribution in the local universe

and because it may have an important influence on the evolution of galaxies (Blanton et al. 2000). The O VI

1032, 1038 absorption line doublet in the spectra of low-redshift QSOs provides a valuable probe of the quantity and properties of this gas, and recent observations with the Space Telescope Imaging Spectrograph on the Hubble Space Telescope have shown that the number of intervening O VI absorbers per unit redshift ( $dN/dz$ ) is quite high (Tripp, Savage, & Jenkins 2000; Tripp & Savage 2000), suggesting that these absorbers do indeed trace a significant baryon repository. In this Letter we use cosmological hydrodynamic simulations to make detailed predictions of the O VI absorption line properties, and we compare these predictions to recent observations. This complements earlier work by Hellsten, Gnedin and Miralda-Escudé (1998), which focused on higher ionization oxygen lines observable with X-ray telescopes.

## 2. SIMULATION

We use two recent cosmological hydrodynamic simulations of the canonical, cosmological constant dominated cold dark matter model (Ostriker & Steinhardt 1995) with the following parameters:  $\Omega_m = 0.3$ ,  $\Omega_b = 0.07$ ,  $h^2 = 0.017$ ,  $h = 0.067$ ,  $\Omega_\Lambda = 0.9$ , and the spectral index of the primordial mass power spectrum  $n = 1.0$ . The higher resolution simulation box has a size of  $25h^{-1} \text{ comoving Mpc}$  on a uniform mesh with  $768^3$  cells and  $384^3$  dark matter particles. The comoving cell size is  $32.6h^{-1} \text{ kpc}$ . The mass of each dark matter particle is  $2.03 \times 10^7 M_\odot$ , and the mean baryonic mass per cell is  $3.35 \times 10^5 h^{-1} M_\odot$ . An earlier simulation with a coarser resolution but a larger box of size  $L = 100h^{-1} \text{ Mpc}$  (Cen & Ostriker 1999a,b) is

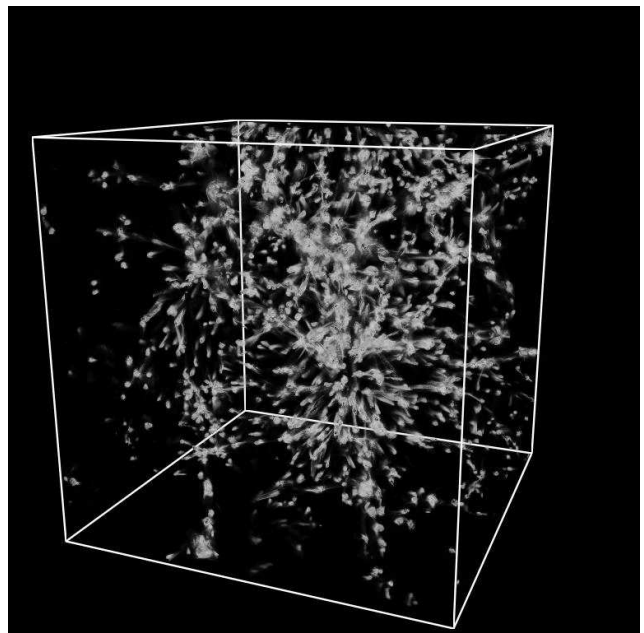
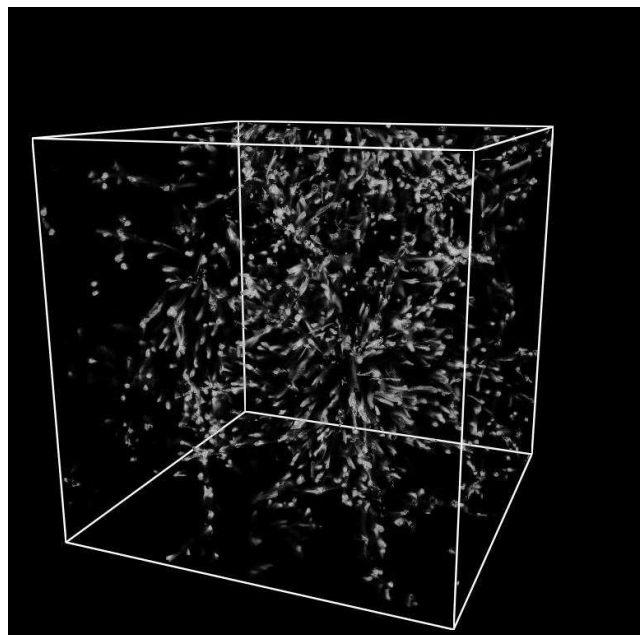
also used to calibrate the boxsize effect. In velocity units the cell sizes are  $\Delta v = (3.3; 19.5)$  km/s in the two simulations, respectively, providing adequate spectral resolution in comparison to current observations.<sup>1</sup>

A word on simulation resolution is relevant here. As simulations with much higher spatial resolutions have shown (Dave et al. 2001), the bulk of the warm-hot intergalactic medium has an overdensity of  $10^{-4}$  to  $10^{-3}$ . This has important implications: the WHIM gas is mostly in uncollapsed regions, for which the Jeans mass is well resolved by our high resolution simulation. In fact, even for a lower temperature, photoionized gas at  $T = 10^4$  K, the Jeans mass is  $10^9 M_\odot$  and Jeans length is 400 kpc/h comoving, which are to be compared to the  $3.3 \times 10^5 M_\odot$  and  $2 \times 10^7 M_\odot$  nominal baryonic and dark matter mass resolution, and 33 kpc/h comoving nominal spatial resolution of our 25 Mpc/h box; the corresponding numbers for our 100 Mpc/h box are  $7.1 \times 10^7 M_\odot$  and  $5.1 \times 10^9 M_\odot$ , and 195 kpc/h. The true spatial and mass resolutions of the simulation are probably a factor of 2 and 8 times worse (Cen & Ostriker 1999b). Clearly, our higher resolution simulation is adequate for resolving unvirialized intergalactic gas that was initially photoionized and then shock heated to the indicated temperature. Our lower resolution simulation is marginal at resolving smaller WHIM structures, which will be evident in the results shown below.

We follow star formation and feedback using a well defined prescription similar to that of other investigators. A stellar particle of mass  $m_{\text{star}} = c m_{\text{gas}} \Delta t$  is created, if the gas in a cell at any time meets the following three conditions simultaneously: (i) slow contracting, (ii) cooling time less than dynamical time, and (iii) Jeans unstable, where  $\Delta t$  is the time step,  $t = \max(t_{\text{dyn}}; 10^7 \text{ yrs})$ ,  $t_{\text{dyn}}$  is the dynamical time of the cell,  $m_{\text{gas}}$  is the baryonic gas mass in the cell and  $c = 0.25$  is star formation efficiency. Each stellar particle has a number of other attributes at birth, including formation time and initial gas metallicity. The typical mass of a stellar particle is one million solar masses. Stellar particles are subsequently treated dynamically as collisionless particles, except that feedback from star formation is allowed in three forms: UV ionizing field, supernova kinetic energy, and metal enriched gas, all being proportional to the local star formation rate. Metals are ejected into the local gas cells where stellar particles are located using a yield  $Y = 0.02$  (Amett 1996) and are followed as a separate species adopting the standard solar composition. The simulation also includes cooling/heating processes due to the self-consistently produced metals using a code based on the Raymond-Smith code assuming ionization equilibrium (Cen et al. 1995). We find that the computed metallicity distributions over a wide range of environments, including clusters of galaxies, damped Lyman systems, Lyman alpha forest and stars, are in broad agreement with observations (Cen & Ostriker 1999c; Nagamine et al. 2001; Cen et al. 2001), lending us confidence that the computed metal distribution in the intermediate regions under consideration (between Lyman alpha forest and clusters of galaxies) may be a good approximation to the real universe.

Post-simulation the photoionization code CLOUDY

(Ferland et al. 1998) is used to compute the abundance of O VI, adopting the shape of the UV background calculated by Haardt & Madau (1996) normalized by the intensity at 1 Ryd determined by Shull et al. (1999) and assuming ionization equilibrium. We generate synthetic absorption spectra using a code similar to that used to generate the synthetic Lyman alpha forest spectra in earlier papers (Cen et al. 1994; Miralda-Escudé et al. 1996). To elucidate the physical nature of the absorbers, we distinguish between photoionized and collisionally ionized gas; O VI absorption lines with optical depth-weighted temperature less than  $10^5$  K are identified as photoionized systems and others as collisionally ionized lines. However, in some cases both ionization mechanisms are important.



<sup>1</sup> The STIS observations reported by Tripp et al. 2000 and Tripp & Savage 2000 have spectral resolution of 7 km/s (FWHM).

Fig. 1. Three-dimensional distribution of the O VI density for photoionized gas (top panel) and collisionally ionized gas (bottom panel). The box size is  $25h^{-1} \text{ Mpc}$ . The color scheme is as follows: light green, green, bright green, green-yellow, yellow, yellow-red and red-black regions have O VI densities of  $10^{-7}$ ,  $10^{-6.5}$ ,  $10^{-6}$ ,  $10^{-5.5}$ ,  $10^{-5}$ ,  $10^{-4.5}$  and  $> 10^{-4.5}$  in units of  $\rho_{\text{crit}}$ .

### 3. RESULTS

Figure 1 shows the 3-d distribution of the O VI density: Figure 1a shows the photoionized O VI and Figure 1b shows the collisionally ionized O VI. It is seen that the low density (bright green) O VI gas is somewhat connected to form a filamentary structure, while higher density gas surrounds roundish regions. Galaxies usually sit in the middle of the roundish red regions (Cen & Ostriker 1999c). The O VI lines due to photoionized gas tend to stem from lower density regions. As we will show later, the bright-green and green-yellow regions produce most of the observed O VI absorption lines; these regions have overdensities of 10–40 times the average density.

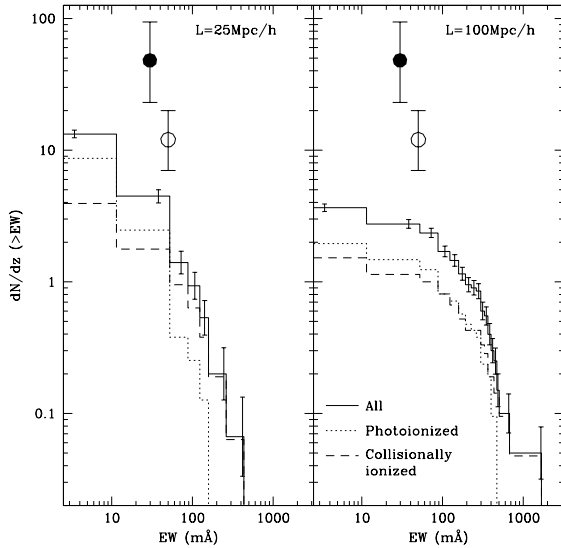


Fig. 2. Cumulative number of O VI absorption lines per unit redshift as a function of the O VI absorption line equivalent width for all lines (solid curve), lines due to photoionized gas (dotted curve) and lines due to collisionally ionized gas (dashed curve) with 1 statistical errorbars. The left panel is from the  $L = 25h^{-1} \text{ Mpc}$  box and the right panel is from the  $L = 100h^{-1} \text{ Mpc}$  box. The equivalent widths are computed by integrating the flux spectrum between downcrossing and upcrossing points at 80% of the continuum. Both dotted and dashed curves are shifted downward by 5% for clarity. The symbols are observational data from Tripp, Savage, & Jenkins (2000; solid dot) and Savage et al. (2001; open dot) with 1 errorbars.

Figure 2 shows cumulative number of lines per unit redshift as a function of the O VI absorption line equivalent width for all lines (solid curve), photoionized lines (dotted curve) and collisionally ionized lines (dashed curve), compared to observations from Tripp et al. (2000) and Savage et al. (2001). We note that at  $\text{EW} < 35 \text{ mÅ}$  the photoionized lines outnumber the collisionally ionized lines. But at the high end of EW the collisionally ionized lines dominate in total numbers of lines, due to the fact that high EW lines originate only in high temperature and higher density regions. Visual examinations of synthetic

O VI absorption spectra indicate that O VI absorption lines due to photo-ionized gas are typically narrower (b parameter) than O VI absorption lines due to collisionally ionized gas. The agreement between simulations and observations is reasonably good, given the small observational samples and computational issues which may have caused both boxes to underestimate the number of lines at various equivalent widths. The larger simulation box (right panel) definitely underestimates the number of lines at  $\text{EW} = 70 \text{ mÅ}$  due to inadequate resolution, while even the smaller box may be underestimating the number of lines at  $\text{EW} = 20 \text{ mÅ}$  and still higher spatial resolution (in progress) would be required to adequately model these lines. But, at larger width, cosmic variance is substantial and the smaller box underestimates the abundance of lines with  $\text{EW} = 350 \text{ mÅ}$ . We argue that a box of size  $L > 100 \text{ Mpc}/h$  may be required, if one is interested in studying lines with  $\text{EW} = 350 \text{ mÅ}$ . We expect that improvement of numerical simulations will likely increase the computed number of lines at both ends of the equivalent width distribution. Recently, Fang & Bryan (2001) have independently obtained very similar results from a cosmological simulation which employs different numerical methods.

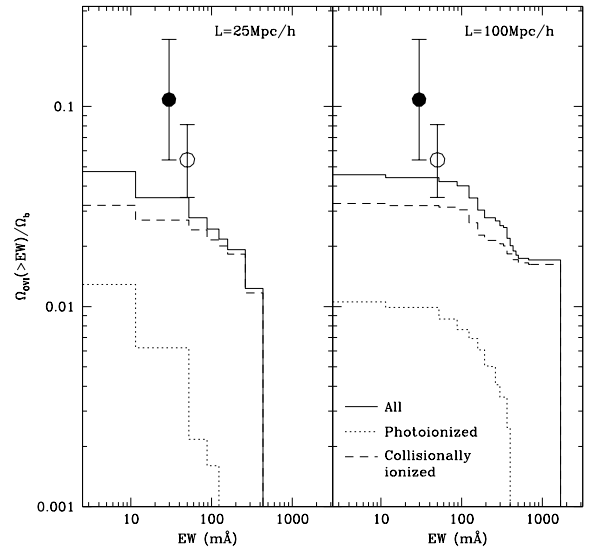


Fig. 3. Cumulative distributions of the fraction of baryonic gas contained in O VI absorption lines, again, for all lines (solid curve), lines due to photoionized gas (dotted curve) and lines due to collisionally ionized gas (dashed curve). The left panel is from the  $L = 25h^{-1} \text{ Mpc}$  box and the right panel is from the  $L = 100h^{-1} \text{ Mpc}$  box. Both dotted and dashed curves are, again, shifted downward by 5% for clarity. The symbols are observational data from Tripp, Savage, & Jenkins (2000; solid dot) and Savage et al. (2001; open dot) with 1 errorbars, assuming  $\langle Z = Z \rangle f(\text{O VI}) = 0.02$  adopted from simulation (see the bottom panel of Figure 4)

Figure 3 shows the cumulative fraction of baryonic gas density contained in the O VI lines as a function of equivalent width for all lines (solid curve), photoionized lines (dotted curve) and collisionally ionized lines (dashed curve), compared to observational constraints. Apparently, most of the mass probed by O VI lines is in lines that are collisionally ionized, although the photoionized lines are dominant in number. This is because collisionally ionized lines originate in higher density regions (see

Figure 4 below). We see that the baryonic gas contained in O VI lines is about 10% of total baryonic matter or roughly 20–30% of the WHIM. The agreement with observations is good, together with the agreement found in Figure 2 strongly suggesting the existence of the WHIM in the real universe and that the inventory of mass derived from the O VI absorption lines accounts for a significant fraction of WHIM. The remaining 70–80% of the WHIM is likely gas which is too hot or does not contain enough oxygen to be detected via O VI absorption.

Finally, Figure 4 reveals the physical properties of the underlying gas that produces the O VI lines. We see that at  $EW = (35;100)$  mÅ the typical metallicity of the gas that produces O VI absorption lines is  $0.1–0.3 Z_{\odot}$  for both photoionized lines and collisionally ionized lines. The typical overdensity is  $(10–40)$  for both photoionized collisionally ionized lines in the range  $EW = 20–200$  mÅ. Photoionized lines tend to reside at the lower end of the overdensity range at the lower  $EW$  end, but two types converge to a typical overdensity of roughly 40 at the high  $EW$  end under consideration. Evidently, the gas that causes the O VI absorption lines is relatively distant from virialized regions such as galaxies, groups, or clusters of galaxies in truly intergalactic, uncollapsed regions.

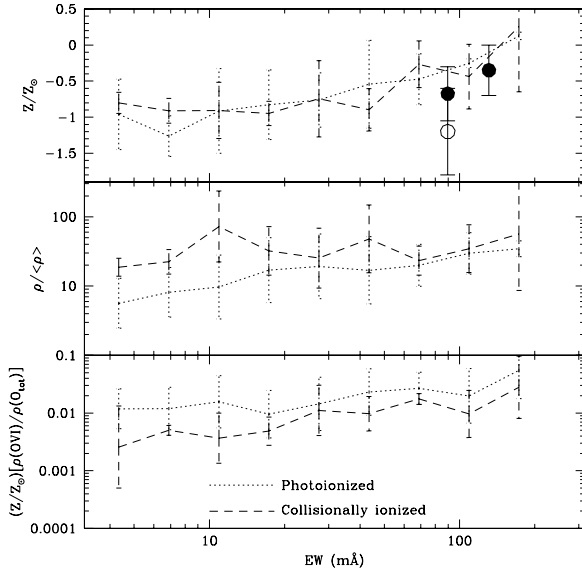


Fig. 4. The physical properties of the underlying gas that produces the O VI lines. The top panel shows metallicity of O VI lines as a function of equivalent width for lines due to photoionized gas (dotted curve) and lines collisionally ionized gas (dashed curve), with 1 dispersion. The symbols are observed metallicities derived by Tripp et al. (2001) and Savage et al. (2001) assuming the gas is photoionized (solid dots) or collisionally ionized (open dots) with 2 errorbars. The middle panel shows the overdensity of regions that produce the O VI absorption lines as a function of equivalent width for lines due to photoionized gas (dotted curve) and due to collisionally ionized gas (dashed curve) with 1 dispersion. The bottom panel shows the product of metallicity and O VI fraction as a function of equivalent width for lines due to photoionized gas (dotted curve) and lines collisionally ionized gas (dashed curve) with 1 dispersion. This quantity is useful for calculating  $\rho_{\text{b}}(\text{O VI})$  from observations, see eqn. 1 of Tripp et al. (2000).

#### 4. DISCUSSION AND CONCLUSIONS

We have made detailed analyses of our latest hydrodynamic simulations to examine the expected properties of O VI absorption lines due to intergalactic gas. In the simulations the vast majority of O VI absorption lines with equivalent width of  $< 35$  mÅ are not due to gas that resides in virialized regions such as galaxies, groups, or clusters of galaxies, but rather due to intergalactic gas of an overdensity of  $10–40$ . These regions form a somewhat connected network of filaments. The typical metallicity of these regions is  $0.1–0.3 Z_{\odot}$ . A relevant test for this contribution is to check in both the real and simulated sky: what is the distance between O VI absorption systems and bright galaxies?

We find that the simulation results agree well with observations with regard to the line abundance and total mass contained in these systems. At O VI absorption line equivalent width of  $< 35$  mÅ one expects to see 5 lines per unit redshift. The number of lines decreases rapidly towards larger equivalent width, dropping to about 0.5 per unit redshift at  $> 35$  mÅ, above which our current simulations may be significantly underestimating the line abundance. About 10% of total baryonic matter or 20–30% of WHIM is expected to be in the O VI absorption line systems with equivalent width  $< 20$  mÅ. Clearly, a larger observational sample of O VI absorption lines would be highly desirable to increase the statistical accuracy as well as other independent observations including absorption lines due to other species and direct emission measurements.

The evolution of WHIM is likely a function of cosmological models, and to some extent, parallels the evolution of clusters of galaxies thus provides a powerful, independent test of cosmological models. The model appears to be qualitatively consistent with the latest observations at higher redshifts (Reimers et al. 2001). We will explore this issue of evolution of WHIM quantitatively in a separate paper.

RC and JPO acknowledge support for this research by NASA grant NAG 5-2759 and NSF grants AST 93-18185, ASC 97-40300 and TMT and EBJ acknowledge support for this research from NASA through grants G0-08165.01-97A and G0-08695.01-A from the Space Telescope Science Institute. We thank the referee for bringing up an important issue regarding the numerical resolution, which helped us more clearly state the relevant effects.

## REFERENCES

- Amett, D. 1996, "Supernovae and Nucleosynthesis", Princeton University Press (Princeton, NJ)
- Blanton, M., Cen, R., Ostriker, J.P., Strauss, M.A., & Tegmark, M. 2000, *ApJ*, 531, 1
- Burles, S., & Tytler, D. 1998, *ApJ*, 499, 699
- Cen, R., Kang, H., Ostriker, J.P., & Ryu, D. 1995, *ApJ*, 451, 436
- Cen, R., & Ostriker, J.P. 1999a, *ApJ*, 514, 1
- Cen, R., & Ostriker, J.P. 1999b, *ApJ*, 517, 31
- Cen, R., & Ostriker, J.P. 1999c, *ApJ*, 519, L109
- Cen, R., Kang, H., Ostriker, J.P., & Ryu, D. 1995, *ApJ*, 451, 436
- Cen, R., Miralda-Escude, J., Ostriker, J.P., & Rauch, M. 1994, *ApJ*, 437, L9
- Cen, R., et al. 2001, in preparation
- Dave, R., Cen, R., Ostriker, J.P., Bryan, G.L., Hemquist, L., Katz, N., Weinberg, D.H., Norman, M.L., & O'Shea, B. 2001, *ApJ*, 552, 473
- Fang, T., & Bryan, G.L. 2001, *ApJ*, submitted
- Ferland, G.J., Korista, K.T., Verner, D.A., Ferguson, J.W., Kingdon, J.B., & Verner, E.M. 1998, *PASP*, 110, 761
- Fukugita, M., Hogan, C.J., & Peebles, P.J.E. 1998, *ApJ*, 503, 518
- Haardt, F., & Madau, P. 1996, *ApJ*, 461, 20
- Hellsten, U., Gnedin, N.Y., & Miralda-Escude, J. 1998, *ApJ*, 509, 56
- Nagamine, K., Fukugita, M., Cen, R., & Ostriker, J.P. 2001, preprint, astro-ph/0011472
- Miralda-Escude, J., Cen, R., Ostriker, J.P., & Rauch, M. 1996, *ApJ*, 471, 582
- Ostriker, J.P., & Steinhardt, P. 1995, *Nature*, 377, 600
- Penton, S.V., Shull, J.M., & Stocke, J.T. 2000, *ApJ*, 544, 150
- Rauch, M., Miralda-Escude, J., Sargent, W.L.W., Barlow, T.A., Weinberg, D.H., Hemquist, L., Katz, N., Cen, R., Ostriker, J.P., 1998, *ApJ*, 489, 1
- Reimers, D., Baade, R., Hagen, H., & Lopez, S. 2001, *A&A*, 374, 871
- Savage, B.D., Sembach, K.R., Tripp, T.M., & Richter, P. 2001, *ApJ*, submitted
- Shull, J.M., et al. 1999, *AJ*, 118, 1450
- Tripp, T.M., Savage, B.D., & Jenkins, E.B. 2000, *ApJ*, 534, L1
- Tripp, T.M., & Savage, B.D. 2000, *ApJ*, 542, 42
- Tripp, T.M., Giroux, M.L., Stocke, J.T., Tumlinson, J., & Oegerle, W.R. 2001, *ApJ*, in press
- Weinberg, D.H., Miralda-Escude, J., Hemquist, L., Katz, N. 1997, *ApJ*, 490, 564